Exogenous alpha-Synuclein decreases raft partitioning of Cav2.2 channels inducing dopamine release

Cellular/Molecular

Exogenous α-Synuclein Decreases Raft Partitioning of $Ca_v2.2$ Channels Inducing Dopamine Release

Giuseppe Ronzitti,[1] Giovanna Bucci,[2] Marco Emanuele,[1] Damiana Leo,[1] Tatyana D. Sotnikova,[1] Liudmila V. Mus,[1] Camille H. Soubrane,[2] Mark L. Dallas,[2] Agnes Thalhammer,[1] Lorenzo A. Cingolani,[1] Sumiko Mochida,[3] Raul R. Gainetdinov,[1,4] Gary J. Stephens,[2] and Evelina Chieregatti[1]

[1]Department of Neuroscience and Brain Technologies, Istituto Italiano di Tecnologia, 16163, Genoa, Italy, [2]School of Pharmacy, University of Reading, Whiteknights, Reading, RG6 6AJ, United Kingdom, [3]Department of Physiology, Tokyo Medical University, Tokyo 160-8402, Japan and [4]Skolkovo Institute of Science and Technology Skolkovo, Moscow region, 143025 and Faculty of Biology and Soil Science, St. Petersburg State University, St. Petersburg, 199034, Russia

α-Synuclein is thought to regulate neurotransmitter release through multiple interactions with presynaptic proteins, cytoskeletal elements, ion channels, and synaptic vesicles membrane. α-Synuclein is abundant in the presynaptic compartment, and its release from neurons and glia has been described as responsible for spreading of α-synuclein-derived pathology. α-Synuclein-dependent dysregulation of neurotransmitter release might occur via its action on surface-exposed calcium channels. Here, we provide electrophysiological and biochemical evidence to show that α-synuclein, applied to rat neurons in culture or striatal slices, selectively activates $Ca_v2.2$ channels, and said activation correlates with increased neurotransmitter release. Furthermore, *in vivo* perfusion of α-synuclein into the striatum also leads to acute dopamine release. We further demonstrate that α-synuclein reduces the amount of plasma membrane cholesterol and alters the partitioning of $Ca_v2.2$ channels, which move from raft to cholesterol-poor areas of the plasma membrane. We provide evidence for a novel mechanism through which α-synuclein acts from the extracellular milieu to modulate neurotransmitter release and propose a unifying hypothesis for the mechanism of α-synuclein action on multiple targets: the reorganization of plasma membrane microdomains.

Key words: **$Ca_v2.2$ channels; dopamine release; extracellular alpha-synuclein; lipid rafts**

Introduction

α-Synuclein (Syn), an unfolded soluble cytosolic protein, has been reported to accumulate in Lewy bodies, which are intraneuronal aggregates pathognomonic of Parkinson's disease (PD) (Spillantini et al., 1997). Although the aggregation pathways and the toxicity of aggregated forms of Syn have been studied extensively, little is known about the role of monomeric Syn in the early phases of PD. Syn is highly enriched in presynaptic terminals, but a substantial fraction of this protein is released in extracellular fluids in healthy and PD subjects (Borghi et al., 2000; El-Agnaf et al., 2003). Importantly, healthy dopaminergic grafts implanted in the striatum undergo degeneration accompanied by Syn-containing Lewy bodies (Kordower et al., 2008a,b), suggesting a potential role of secreted extracellular Syn in the onset of the disorder. Although the direct transfer of Syn between neurons has been demonstrated (Hansen et al., 2011; Volpicelli-Daley et al., 2011), little is currently known about the process of release of Syn and its physiopathological function. Duplications and triplications of the *SNCA* gene encoding α-synuclein are present in familial forms of PD. Recently, the *SNCA* gene was identified as a risk locus in genome-wide association studies for PD, highlighting the importance of wild-type Syn levels as pathogenic factor also in the sporadic form of PD (Satake et al., 2009; Venda et al., 2010).

Maintenance of calcium homeostasis through the regulation of presynaptic calcium channels and intracellular calcium stores is fundamental for correct synaptic activity. Calcium dyshomeostasis has been proposed recently as the primary age-related condition driving neurodegeneration in the sporadic form of PD, in which selective subpopulations of neurons undergo degeneration. Dopaminergic neurons expressing higher levels of calcium binding proteins, such as calbindin, calretinin, and parvalbumin, seem to be resistant to degeneration in PD (Damier et al., 1999; Kim et al., 2000; Soós et al., 2004). Dysfunction in the ion channels and receptors regulating synaptic communication may contribute to the cognitive decline, neurological and motor symptoms associated with chronic disorders (Walsh and Selkoe,

Received Feb. 12, 2014; revised June 11, 2014; accepted June 27, 2014.

Author contributions: G.R., G.B., R.R.G., and E.C. designed research; G.R., G.B., M.E., D.L., T.D.S., L.V.M., C.H.S., M.L.D., A.T., and S.M. performed research; G.R., G.B., M.E., D.L., L.A.C., S.M., R.R.G., G.J.S., and E.C. analyzed data; G.J.S. and E.C. wrote the paper.

This work was supported by Telethon Foundation Grant GGP10109 (E.C.). We thank B. Lauring (Columbia University, New York, NY) for Syn plasmid and S.M. Voglmaier (University of California, San Francisco, San Francisco, CA) for SyGCaMP3 plasmid.

The authors declare no competing financial interests.

Correspondence should be addressed to Evelina Chieregatti, Department of Neuroscience and Brain Technologies, Istituto Italiano di Tecnologia, via Morego 30, 16163, Genova, Italy. E-mail: evelina.chieregatti@iit.it.

G. Ronzitti's present address: Genethon, Evry, 91000 France.

G. Bucci's present address: Department of Physics, University of Oxford, Oxford, OX1 3PU, UK.

DOI:10.1523/JNEUROSCI.0608-14.2014

 0270-6474/14/3410603-13$15.00/0

2004; Mattson, 2007). In neurons, presynaptic voltage-gated calcium channels (Ca_v) 2.1 and $Ca_v2.2$ are predominantly responsible for coupling neuronal depolarization to neurotransmitter release. In particular, $Ca_v2.2$ underlie dopamine (DA) release in the basal ganglia (Bergquist et al., 1998). In SH-SY5Y cells, an increase in calcium influx through Ca_v has been suggested to be caused by increased expression of Syn or by extracellular Syn (Hettiarachchi et al., 2009; Melachroinou et al., 2013). In synaptoneurosomes, an increase in calcium influx through $Ca_v2.2$ occurs during incubation with micromolar Syn concentrations; such an effect occurred independently of free radical generation and was suggested to arise through a direct interaction of Syn with $Ca_v2.2$ (Adamczyk and Strosznajder, 2006). Mouse models of Syn-induced neurodegeneration exhibit a decreased DA release, similar to that observed in PD patients (Decressac et al., 2012; Lundblad et al., 2012; Nuber et al., 2013). However, increased tonic DA levels attributable to early synaptic dysfunction, preceding the death of dopaminergic neurons and leading to a possible disruption of corticostriatal transmission (Wu et al., 2010), were found in Syn transgenic mice at a young age (Lam et al., 2011), similar to that assessed in other PD models (Goldberg et al., 2003).

Here we evaluate the alteration of synaptic activity attributable to the presence of raised concentrations of Syn in the extracellular space. We analyze in detail the effect of extracellularly applied monomeric Syn on depolarization-evoked calcium influx and $Ca_v2.2$ calcium current density in neurons and on neurotransmitter release *in vitro* and *in vivo*, identifying the molecular mechanism of Syn action as a decrease in raft partitioning of $Ca_v2.2$ to induce DA release. Such a Syn regulatory mechanism may have important consequences in PD and related synucleopathies.

Materials and Methods

Reagents

All chemicals, unless otherwise stated were purchased from Sigma-Aldrich. The following primary antibodies were used: anti-Cav2.2 α1B (A-11; Santa Cruz Biotechnology catalog #sc-271010, RRID:AB_10611357), anti-G-protein β1 (C-16; Santa Cruz Biotechnology catalog #sc-379, RRID:AB_2111823), anti-α2δ1 subunit (Santa Cruz Biotechnology catalog #sc-133436, RRID:AB_10609764), anti-Hsp90 (Santa Cruz Biotechnology catalog #sc-59578, RRID:AB_2295578), anti-flotillin-1 (BD Biosciences catalog #610821, RRID:AB_398140), anti-caveolin-1 (BD Biosciences catalog #610059, RRID:AB_397471), anti-α-synuclein (BD Biosciences catalog #610787, RRID:AB_398108), anti-Na^+/K^+ ATPase (EMD Millipore catalog #05-369, RRID:AB_309699), anti-Ca_v-β2 subunit (Sigma-Aldrich catalog #C5738, RRID:AB_258910), anti-synaptophysin (Synaptic Systems catalog #101 011, RRID:AB_887824), anti-syntaxin 1A antibody (Santa Cruz Biotechnology catalog #sc-58299, RRID:AB_785887), anti-Rab11 (Life Technologies catalog #700184, RRID:AB_10562415), and anti-$Ca_v1.2$ (Hell et al., 1996). Syn peptides (amino acids 12–23, 34–45, and 61–78) were obtained from Primmbiotech.

Rat primary cortical cultures

All experiments were performed in accordance with the Italian Ministry of Health. Primary cultures of rat embryonic cortical neurons were prepared as described previously (Brewer, 1997). Briefly, E18 Sprague Dawley rat embryos (Charles River) were decapitated, and cortices were rapidly dissected and dissociated by incubation in Neurobasal medium (Life Technologies) containing 20 U/ml papain, 1.1 mg/ml cysteine, and 125 μg/ml DNase for 30 min at 37°C. After cell dissociation, cortical neurons were plated in either six-well dishes at a density of 1×10^6 cells/ml on glass coverslips coated with poly-L-lysine (0.1 μg/ml) or 100 mm Petri dishes coated with poly-L-lysine (0.01 μg/ml) at a density of 5×10^6 cells per dish. Cells were cultured in Neurobasal medium supplemented with B-27, GlutaMAX, and penicillin–streptomycin (all from Life Technologies) and maintained at 37°C in 5% CO_2. In all experiments, neurons were used between 7 and 14 d *in vitro* (DIV).

Syn purification

The construct encoding the full-length human wild-type Syn inserted in the pET21d plasmid was a kind gift from Dr. B. Lauring (Columbia University, New York, NY). Purification was performed as described previously (Martinez et al., 2003). Bacteria were induced during the exponential phase with 1 mM isopropyl β-D-1-thiogalactopyranoside for 2 h and harvested by centrifugation. The pellet was solubilized in 20 mM HEPES/KOH, pH 7.2, and 100 mM KCl (buffer A) and heated for 5 min at 90°C. The cell lysate was centrifuged at 72,000 × *g* for 30 min, and the supernatant was loaded on a HiTrap monoQ column (GE Healthcare). Syn was eluted with a liner gradient of KCl from 100 to 500 mM, and the fractions of interest were concentrated using a Centricon centrifugal filter (Millipore) before loading on a Superose 12 column in buffer A (GE Healthcare). The fractions containing Syn were pooled, concentrated, and stored at −80°C. To control Syn purity, 1 mg of purified Syn was loaded on top of a Superdex 75 10/300 column (GE Healthcare) and eluted at 0.5 ml/min on an AKTA Purifier apparatus. Optical density (OD) was continuously measured at 280 nm.

Lipid raft isolation

All procedures were performed at 4°C. Lipid raft isolation was performed on cortical neurons at 10 DIV as described previously (Butchbach et al., 2004). Briefly, primary cortical neurons (5×10^6 neurons per dish) were incubated for 1 h at 4°C with 80 μl/dish PBS containing 1% of Triton X-100 and Complete Mini protease inhibitor (Roche Applied Science). The extract was added with sucrose to obtain a 40% final concentration. A total of 900 μl of the extract was placed on the bottom of an ultracentrifugation tube, and a discontinuous 5–30% sucrose gradient was formed on top of the extract. The gradient was then centrifuged at 47,000 rpm for 16 h at 4°C using a MLS 50 rotor (Beckman Coulter). Ten 0.5 ml fractions were collected from the top of each gradient. A total of 400 μl of the sample was added to 100 μl of 5× SDS-PAGE loading buffer (100 mM Tris, pH 7.5, 7.5 mM EDTA, 10% SDS, 10% β-mercaptoethanol, 50% glycerol, and 0.02% bromophenol blue).

Biotinylation procedure

The entire biotinylation procedure was performed at 4°C. Labeling of proteins of the plasma membrane was achieved by biotinylation of cortical neurons (10 DIV) and was a slight modification of the protocol reported previously (Butchbach et al., 2004). The cells were washed twice in PBS and once in HBSS and then incubated in HBSS containing 0.6 mg/ml EZ-link Sulfo-NHS-biotin (Thermo Fisher Scientific) for 15 min. The cells were then incubated in quenching buffer (5% BSA in HBSS) for 10 min, scraped, and recovered by centrifugation. Cell pellets were incubated for 1 h with constant shaking in PBS containing 1% Triton X-100 and Complete Mini protease inhibitor (Roche Applied Science). The biotinylated extract was separated in a sucrose gradient (as described above), the fraction was collected, and SDS was added to a final 0.5%. The biotinylated proteins present in each fraction were pulled down by incubation with 100 μl of Neutravidin beads (50% slurry; Thermo Fisher Scientific) for 2 h. Avidin beads were then recovered by centrifugation and washed four times in PBS. After washing, bound proteins were eluted with 1× SDS-PAGE loading buffer (20 mM Tris, pH 7.5, 1.5 mM EDTA, 2% SDS, 2% β-mercaptoethanol, 10% glycerol, and 0.004% bromophenol blue).

Immunoblot analysis

SDS-PAGE and electrotransfer of membranes were performed as described previously (Laemmli, 1970). Immunoreactive bands were detected by chemiluminescence, and images were acquired using an LAS AF 4000 apparatus (GE Healthcare). Bands intensities were measured by Image Quant analysis software (GE Healthcare).

Filipin quantitative staining

Filipin quantitative staining of fixed cells was performed accordingly to a modification of a commercially available kit (catalog #10009779; Cayman Chemicals). Briefly, cortical neurons (10 DIV) plated on 18 mm

coverslips were fixed with 4% (v/v) PFA, washed in PBS, and incubated for 1 h in PBS containing 1% Triton X-100 (filipin total staining) or PBS (filipin membrane staining). Next, coverslips were incubated for 1 h at room temperature in 30 μl of PBS and 10% NGS (Thermo Fisher Scientific), containing 100 μg/ml filipin [freshly prepared from a 10 mg/ml stock solution (in EtOH) stored at −20°C]. Finally, coverslips were incubated for 30 min at room temperature in 500 μl of 1% SDS, and the fluorescence of the solution was measured on a LS55 fluorometer (PerkinElmer Life and Analytical Sciences).

Fluo-4 imaging

Rat embryonic cortical neurons were plated onto 25 mm coverslips at a density of 800 neurons/mm^2 and at 6–10 DIV were incubated with buffer A or 5 μM Syn for 2 h at 37°C. Neurons were then loaded with Fluo-4-AM (2.5 μM; Life Technologies) for 20 min at 37°C. Coverslip were then transferred into a perfusion chamber (Warner Instruments) and superfused with modified Krebs' solution containing the following (in mM): 135 NaCl, 5 KCl, 1.5 $CaCl_2$, 0.75 $MgCl_2$, 0.75 KH_2PO_4, 1.5 $MgSO_4$, 5.6 glucose, and 20 Na-HEPES, pH 7.4 (adjusted with NaOH). NBQX at 10 μM, 50 μM D-APV, and 100 μM picrotoxin were added to the solution. Nifedipine at 10 μM, 300 nM ω-conotoxin GVIA, or 100 nM ω-agatoxin IVA (Bachem) was added as described. Fluo-4 fluorescence was recorded at 494 ± 10 nm wavelength at 1 Hz for 3 min. Basal fluorescence was recorded for 1 min, and then Ca^{2+} entry was elicited by a 60 s bath application of a modified Krebs' solution containing 50 mM KCl with a reciprocal decrease in Na^+ concentration. A single stimulation was performed per coverslip. Results were expressed as the ratio between the basal fluorescence and the maximum fluorescence of the neurons during 50 mM KCl stimulation (F/F_0). F/F_0 ratio was normalized for each experiment to the respective control. Calcium imaging was performed on a Leica AF6000 microscope to acquire images at 1 frame/s.

GCaMP3 imaging

Rat embryonic cortical neurons were plated at a density of 400 neurons/mm^2 and at 10 DIV were transfected with SyGCaMP3 (GCaMP3 with synaptophysin; Niwa et al., 1991; kindly provided by Dr. Susan Voglmaier, University of California, San Francisco, San Francisco, CA) using calcium phosphate. At 13 DIV, cells were treated with buffer A or 5 μM Syn for 2 h at 37°C. Imaging was performed as described above using the same acquisition and stimulation conditions. Data were analyzed with the NIH ImageJ plugin Time Series analyzer 2.0. After subtraction of the first image from the image obtained during the peak of stimulation with 50 mM KCl and application of a threshold to obtain a binary image, boutons were identified using the NIH ImageJ Analyze Particles software to detect regions of interest (ROIs).

Electrophysiology

Superior cervical ganglia neurons for patch-clamp recordings. Superior cervical ganglia neurons (SCGNs) were acutely dissected from 3- to 6-week-old male Wistar rats according to the guidance of the UK Animals (Scientific Procedures) Act 1986 subject to University of Reading Local Ethic Research Panel review, as described previously (Bucci et al., 2011). Briefly, SCG were dissected and placed in cold L-15 medium (Sigma Aldrich) containing 5% penicillin–streptomycin (Life Technologies). The ganglia were then acutely dissociated in DMEM containing 0.5 mg/ml trypsin, 1 mg/ml collagenase, and 3.6 mg/ml glucose (all from Sigma Aldrich). After incubation at 37°C for 30–40 min, the digestion reaction was stopped by the addition of 84% Eagle's MEM, 10% fetal calf serum, 5% horse serum (Lonza), and 1% penicillin–streptomycin (Gibco Invitrogen). After dissociation, cells were plated onto coverslips coated with poly-L-ornithine (Sigma-Aldrich) and incubated at 37°C (5% CO_2) before electrophysiological recordings.

Whole-cell voltage-clamp recordings. Whole-cell recordings from isolated SCGNs were performed as described previously (Bucci et al., 2011) using borosilicate glass electrodes with resistances between 5 and 7 MΩ when filled with an intracellular solution [in mM: 140 CsCl, 10 HEPES, 0.1 $CaCl_2$, 1.0 $MgCl_2$, 4 Mg-ATP, 0.2 Na-GTP, and 1.0 EGTA, pH 7.3 (adjusted with CsOH)] and an extracellular solution [in mM: 160 tetraethylammonium bromide, 10 HEPES, 3 KCl, 1 $MgCl_2$, and 4 glucose, with 10 mM Ba^{2+} as charge carrier, pH 7.4 (adjusted with Sigma 7–9 base)]. Membrane currents were acquired at a holding potential (V_h) of −70 mV using an Axopatch 200B patch-clamp amplifier and WinWCP version 4.0.7 software (John Dempster, University of Strathclyde, Glasgow, UK). Linear components of capacitive and leak currents were subtracted using the standard P/4 protocol. Series resistance compensation of >70% was typically used. Data were analyzed offline using WinWCP version 4.0.7, OriginPro version 7.0 (Microcal), and MATLAB (MathWorks) software. *I–V* data were fitted with the modified Boltzmann equation:

$$\text{current density: } G_{max}(V - V_{rev})/(1 + \exp(V - V_{0.5})/k)),$$

where G_{max} is the maximum conductance, V_{rev} is the null potential, $V_{0.5}$ is the voltage at which 50% of the current is activated, and k is the slope factor. To determine $V_{0.5}$ and k values accurately, data from normalized tail current amplitude was fitted with a standard Boltzmann function. Statistical significance (taken as $p < 0.05$) was determined using one-way ANOVA, Student's *t* test, or Mann–Whitney *U* test, as indicated.

Synaptic transmission between SCGNs. Cells were prepared as described previously (Mochida et al., 1996). Briefly, males Wistar rats were decapitated on postnatal day 7 under diethylether anesthesia according to the guidelines of the Physiological Society of Japan. SCGNs were isolated and maintained in culture for 6–7 weeks in a growth medium of 84% Eagle's MEM, 10% fetal calf serum, 5% horse serum, 1% penicillin–streptomycin (all from Life Technologies), and 25 ng/ml nerve growth factor (2.5 S, grade II; Alomone Labs).

Paired intracellular recordings were made from two proximal neurons using microelectrodes filled with 1 M potassium acetate (70–90 MΩ) as described previously (Mochida et al., 2003). Briefly, SCGNs were superfused with modified Krebs' solution containing the following (in mM): 136 NaCl, 5.9 KCl, 2.5 $CaCl_2$, 1.2 $MgCl_2$, 11 glucose, and 3 Na-HEPES, pH 7.4 (adjusted with NaOH). Action potentials (APs) were generated in a neuron by current injection (at 0.1 Hz) through the intracellular recording electrode and EPSPs recorded from the synaptically coupled neuron. Data were analyzed using software written by the late Ladislav Tauc (National Center of Scientific Research, Paris, France). Throughout, data were obtained at 32–35°C. Collected data were analyzed with Origin software (Origin Lab) and are reported as means ± SEMs. Statistical significance (taken as $p < 0.05$) was determined using Student's *t* test.

Fast-scan cyclic voltammetry

Male Wistar rats were anesthetized with halothane and decapitated. The brain was removed, and coronal slices containing the dorsal striatum were cut at a thickness of 300 μm in cold carboxygenated artificial CSF (aCSF; in mM: 125 NaCl, 2.5 KCl, 0.3 KH_2PO_4, 26 $NaHCO_3$, 2.4 $CaCl_2$, 1.3 $MgSO_4$, and 10 D-glucose) using a VT1000S vibrating microtome (Leica Microsystems). Dorsal striatal brain slices were allowed to recover for at least 1 h at room temperature in carboxygenated aCSF. For recordings, slices were superfused with 32°C carboxygenated aCSF at a flow rate of 1 ml/min. Experimental recordings started a minimum of 20 min after transfer to the slice chamber. Carbon fiber electrodes (5 μm; Goodfellow) were made as described previously (Kuhr and Wightman, 1986). Electrodes were inserted ~100 μm into the slice. The potential of the working electrode was held at −0.4 V versus Ag/AgCl between scans and was ramped to +1.3 V at 300 V/s and back at −0.4 V every 100 ms via an A-M Systems isolated pulse stimulator. The triangular waveform was computer controlled using a HEKA EVA8 potensiostat and a ESA Bioscience fast-scan cyclic voltammetry interface analog-to-digital converter via TH-1 software (ESA Biosciences). Axonal DA release in the dorsolateral striatum was evoked using a twisted bipolar stimulating electrode (Plastics One). Stimulations were delivered every 2 min by a single electrical pulse (1 ms, 400 μA). Syn at 5 μM (dissolved in aCSF) was superfused 10 min after the first measure. For ω-conotoxin experiments, drug was superfused (at 1 ml/min) starting from 4 min before the first recording until the end of the experiment. Background-subtracted cyclic voltammograms were obtained by subtracting the current obtained before stimulation from all recordings. The peak oxidation current for DA in each voltammogram was converted into a measure of DA concentration by post-calibration of the electrode using 1 μM DA (Sigma-Aldrich).

Data were normalized to the first five recordings (10 min) of their respective control period and plotted against time (means ± SEMs). Statistical significance (taken as $p < 0.05$) was determined by two-way ANOVA (time × treatment as variables).

Microdialysis

In vitro Syn microdialysis was performed to verify Syn diffusion through the microdialysis membrane. A 4 mm, 100 kDa cutoff membrane (CMA12 guide; CMA Microdialysis) was connected to a microdialysis syringe pump (CMA-402 syringe pump; CMA Microdialysis). aCSF (in mM: 147 NaCl, 2.7 KCl, 1.2 $CaCl_2$, and 0.8 $MgCl_2$) plus 10 μM Syn was used as a perfusion medium at a flow rate of 0.1 μl/min. The microdialysis cannula was immersed in 50 μl of aCSF, and the appearance of Syn in the solution was measured by SDS-PAGE and Western blot performed on 2 μl fractions sampled at the indicated times.

In vivo Syn microdialysis was performed in awake and freely moving rats (males Wistar). A guide cannula (CMA12 guide; CMA Microdialysis) was stereotaxically implanted in the right striatum under isoflurane anesthesia and cemented. Stereotaxic coordinates for probe positioning were chosen according to a rat brain atlas: anteroposterior, +1.0 mm; lateral, 3.0 mm; and dorsoventral, −6.5 mm relative to bregma. Approximately 24 h after surgery, dialysis probes were inserted into the guide cannula. The dialysis probes were perfused during implantation into the brain and for 1 h afterward with aCSF. At 1 h after the operation, animals were returned to their home cages. On the next day, the dialysis probes were connected to a syringe pump and perfused with aCSF at 1.0 μl/min for 30 min (washout period). After this stage, the perfusion rate was changed to 0.25 μl/min, and aCSF was perfused for 2 h (equilibration period). The solution was then changed to aCSF containing buffer A, and perfusion was continued for 3 h at 0.25 μl/min. Samples were collected every 60 min into collection tubes containing 2 μl of perchloric acid (1 M). After the experiment, animals were disconnected from the system and were left in their home cage overnight. On the second day, the dialysis probes were connected again to a syringe pump and perfused according to the protocol described above with addition of aCSF containing Syn (10 μM). The samples collected during hour 3 of Syn or buffer A application were used for analysis. DA content in samples collected with and without Syn application was determined by HPLC.

HPLC analytical procedure

Measurements of DA in microdialysis samples were performed using HPLC with electrochemical detection (ALEXYS LC-EC system) equipped with a reverse-phase column (3 μm particles, ALB-215 C18, 1 × 150 mm; Antec) at a flow rate of 200 μl/min and electrochemically detected by a 0.7 mm glass carbon electrode (VT-03; Antec). The mobile phase contained 50 mM H_3PO_4, 50 mM citric acid, 8 mM KCl, 0.1 mM EDTA, 400 mg/l octanesulfonic acid sodium salt, and 10% (v/v) methanol, pH 3.9. The sensitivity of the method allowed detection of ~3 fmol of DA. Dialysate samples (11 μl) were injected into HPLC without any additional purification.

Results

Extracellular Syn induces an increase in evoked calcium entry through $Ca_v2.2$

Syn has been shown to be released in physiological and pathological conditions *in vitro* and *in vivo*. First, we confirmed the release of Syn from cultured rat neurons over a period of 48 h; Syn was found in the medium in picomolar concentration. Neurons showed no sign of damage or leakage of cytosolic proteins as shown by the absence of GAPDH in the media (Fig. 1*A*). To determine whether extracellular Syn can affect intracellular calcium levels, we applied highly purified Syn to rat cortical neurons (10 DIV). The monomeric state of purified Syn was assessed by gel filtration and SDS-PAGE (Fig. 1*B*). During incubation of the purified protein with cultured neurons, the formation of oligomers was found at 48 h (Fig. 1*C*). The absence of oligomeric or cleaved products of the protein after 2 h incubation was confirmed by gel filtration. Fractions collected from the column

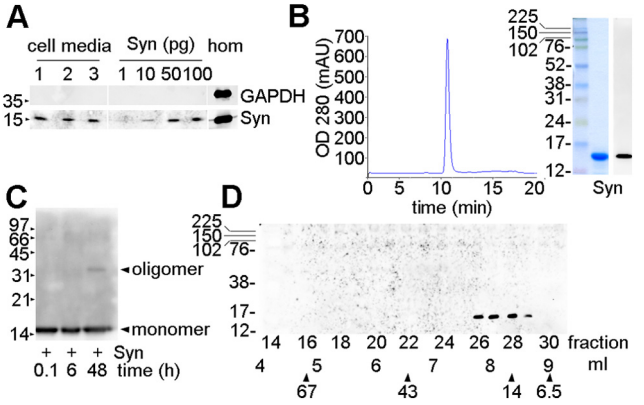

Figure 1. Analysis of released Syn and purified Syn incubated with neurons. ***A***, Immunoblots showing the presence of Syn in the culture media collected from rat cortical neurons at 6, 8, and 10 DIV over a 48 h period, and, in the homogenate (hom) collected at 10 DIV, GADPH was used as a control for membrane leakage. The amount of Syn in the media is in the picomolar range (quantified by densitometry compared with a standard curve of purified Syn). ***B***, Left, FPLC chromatogram of recombinant Syn. OD measured at 280 nm of purified Syn (1 mg) loaded on top of a Superdex 75 10/300 column and eluted a 1 ml/min. Right, Syn (10 μg) was loaded on 13% acrylamide gel and subjected to Coomassie staining (left; rainbow molecular weight markers are indicated) or immunoblotted with anti-Syn antibody. ***C***, Immunoblot of the medium collected from 10 DIV rat cortical neurons incubated with recombinant Syn for 0.1, 6, and 48 h, showing the presence of SDS-resistant higher-molecular-weight Syn products (oligomers) after 48 h. ***D***, Immunoblot of the fractions eluted at 0.5 ml/min from a Superdex 75 10/300 column loaded with the medium collected from 10 DIV rat cortical neurons incubated with recombinant Syn for 2 h. The elution peak of BSA (67 kDa), ovalbumin (43 kDa), ribonuclease A (13.7 kDa), and aprotinin (6.5 kDa), separated under the same conditions, is indicated by each of the arrows.

showed that the bulk of Syn eluted with proteins of 14–20 kDa, as assessed by a calibration column, and indicate that Syn was monomeric (Fig. 1*D*). Neurons were incubated with or without recombinant Syn (5 μM) for 2 h at 37°C and subsequently loaded with the calcium dye Fluo-4 (Fig. 2*A*). In the presence of AMPA and NMDA ionotropic glutamate receptor blockers, we did not detect any significant effect on basal calcium level during Syn application, whereas we measured an ~12% increase in calcium influx after depolarization of neurons with 50 mM KCl (Fig. 2*A*, middle). We evaluated the time course of effects of Syn preincubation and found a significant increase in calcium influx after 30 min, which was higher and more reproducible after 2 h preincubation (Fig. 2*A*, right). We applied nifedipine (10 μM), a selective blocker of Ca_v1, to analyze their possible involvement in Syn action. Under these conditions, we found a significantly larger, (~22%) increase in calcium signal during Syn exposure, suggesting that, in the absence of nifedipine, we could have underestimated the change in fluorescence because of partial dye saturation (Fig. 2*B*, left). To determine which calcium channels are targeted by Syn, we used, in addition to nifedipine, the specific calcium channel inhibitors ω-agatoxin IVA and ω-conotoxin GVIA to block $Ca_v2.1$ and $Ca_v2.2$, respectively (Fig. 2*B*, middle and right). ω-Agatoxin had no effect on Syn-induced increase in calcium entry, whereas ω-conotoxin completely abolished the effect of Syn, indicating that $Ca_v2.2$ are selectively affected by Syn in cortical neurons. Because of the power relationship between calcium influx and exocytosis (Dodge and Rahamimoff, 1967), small changes in influx might have profound effects on transmitter release; however, to exclude the possibility that the effect of Syn could be unspecific, we used three distinct Syn peptides: (1) P34 (amino acids 34–45), i.e., the glycosphingolipid-binding domain of Syn; (2) P61 (amino acids 61–78), i.e., the cholesterol

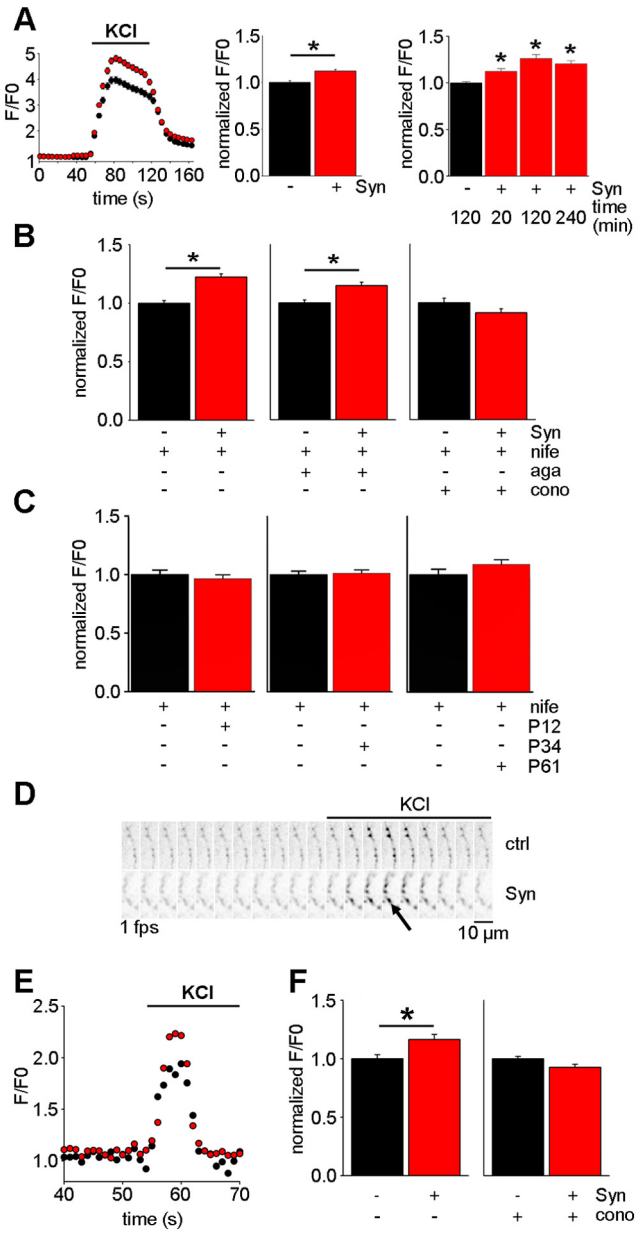

Figure 2. Extracellular Syn increases calcium influx through $Ca_v2.2$. ***A***, Left, Representative trace of a calcium transient of a cortical neuron obtained after perfusion for 60 s with 50 mM KCl (starting point at 60 s). Neurons were incubated with 5 μM Syn (red dots) for 2 h at 37°C or without (black dots); neurons were loaded with Fluo-4 and imaged at 1 frame/s. Data are expressed as F/F_0 (ratio between basal fluorescence in the first 20 s and fluorescence at each data point). Middle, Bar chart showing the increase in fluorescence calculated at the point of maximum value in Syn-treated neurons (red; $n = 150$). Data were pooled from different experiments and normalized to the respective control (black; $n = 150$) in each experiment. Right, Bar chart showing the increase in fluorescence, calculated as above, in neurons treated with 5 μM Syn for 20 min, 2 h, and 4 h (red; $n = 83$, $n = 63$, $n = 67$). Data were normalized to the control (black; $n = 120$) in each experiment. Statistical significance determined by one-way ANOVA. *$p < 0.05$. ***B***, Quantification of Fluo-4 fluorescence during KCl depolarization in Syn-treated neurons (red), calculated as above, in the presence of 10 μM nifedipine (nife; $n = 600$), 100 nM ω-agatoxin (aga; $n = 450$), or 300 nM ω-conotoxin (cono; $n = 250$), each bath applied 3 min before KCl perfusion. Data are expressed as mean ± SEM of F/F_0 normalized to the respective control (black; same n as Syn-treated samples). ***C***, Bar chart showing the increase in fluorescence calculated as above, in neurons treated with 5 μM P12, P34, and P61 Syn peptides for 2 h (red; $n = 150$, $n = 375$, $n = 167$). Data were pooled from different experiments and normalized to the respective control (black; $n = 150$, $n = 376$, $n = 100$) in each experiment. ***D***, Series of microphotographs showing a group of positive synapses (black arrow) in neurons transfected with SyGCaMP3 and depolarized with 50 mM KCl in the presence of nifedipine and in the absence (top) or presence (bottom) of Syn. KCl was perfused starting at frame 12 and caused synaptic boutons to emit fluorescence immediately. ctrl, Control. ***E***, Representative trace of the increase in calcium in neurons transfected with SyGCaMP3 and depolarized as above. Neurons were incubated with 5 μM Syn (red dots) or without (black dots) as in ***A***. Images were acquired at 1 frame/s. ***F***, Left, Quantification of the fluorescence in SyGCaMP3-positive boutons (red; $n = 100$) in Syn-treated neurons normalized to the respective control (black; $n = 100$). Right, Quantification as in the left panel of neurons perfused with 300 nM ω-conotoxin (cono) 3 min before KCl. Data were expressed as the mean ± SEM of F/F_0 normalized to the respective control. Statistical significance in ***A–C*** and ***F*** determined by nonparametric t test. *$p < 0.05$.

binding domain of Syn that has been shown to induce membrane leakage and to aggregate (Crowet et al., 2007; Fantini et al., 2011); and (3) P12 (amino acids 12–23), a peptide with no recognized function. None of these peptides determined measurable effects on calcium entry (Fig. 2*C*), indicating that the whole protein, albeit unfolded, is required for its activity on Cav2.2.

$Ca_v2.2$ are localized presynaptically and are major regulators of neurotransmitter release (Westenbroek et al., 1992; Catterall, 2000; Garner et al., 2000). To investigate the action of extracellular Syn on calcium influx specifically in the presynaptic compartment, the calcium indicator GCaMP3 was targeted to synaptic vesicles as a chimera with the synaptic vesicle associated protein synaptophysin (SyGCaMP3) (Li et al., 2011). In neurons expressing SyGCaMP3, the fluorescent signal in presynaptic boutons was increased during KCl perfusion (Fig. 2*D*). In the selected ROI, fluorescence reached a peak lasting ~7 s (Fig. 2*E*). Incubation of neurons with Syn induced an ~15% increase in calcium entry at the presynapse that was also completely abrogated by ω-conotoxin (Fig. 2*F*), suggesting a possible activity of extracellular Syn in the regulation of neurotransmitter release by $Ca_v2.2$.

Extracellular Syn increases whole-cell $Ca_v2.2$ current density and synaptic transmission in isolated SCGNs

Rat SCGNs were used to measure the Syn effect on $Ca_v2.2$ activity because, in these neurons, 85% of calcium current is carried by ω-conotoxin-sensitive $Ca_v2.2$ (Stoehr et al., 1997). Whole-cell calcium currents (measured as I_{Ba}) in SCGNs cultured 1–2 d were assessed after 2 h preincubation with purified recombinant Syn at various concentrations (Fig. 3*A*, representative traces in center panel). The modulatory effect of Syn was measured against separate pools of internal control recordings from SCGNs within the same preparation. Pretreatment of neurons with 5 μM Syn in the culture medium caused an ~70% increase in calcium current density at 0 mV and a corresponding increase in G_{max} (Fig. 3*A*; Table 1). In these experiments, control Syn had no significant effect on V_{rev} (Table 1). At a 10 times lower concentration (0.5 μM), Syn also produced a significant increase of calcium current density and G_{max} with no significant difference between the two concentrations tested, whereas 0.1 μM Syn, the lowest concentration applied, failed to produce any significant effect compared with controls (Fig. 3*A*, right; Table 1). To investigate the effect of Syn on $V_{0.5}$ and slope factor (k), we fitted Boltzmann functions to tail current amplitude data measured at −120 mV; these protocols use short activation pulses to avoid any contaminating voltage-dependent current inactivation and so give the most accurate measures of transition between closed and open states. Concentrations of Syn that affected current density and G_{max} had no effect on $V_{0.5}$, but caused a significant decrease in k values (Table 2). The reduction in k suggests that Syn improves the movement of gating charges and, thus, facilitates transition from a closed to open state that occurred over a smaller voltage range in Syn-modified channels. In addition, Syn had no effect on steady-state inactivation $V_{0.5}$ and slope factor k (see Fig. 5*D*); these data

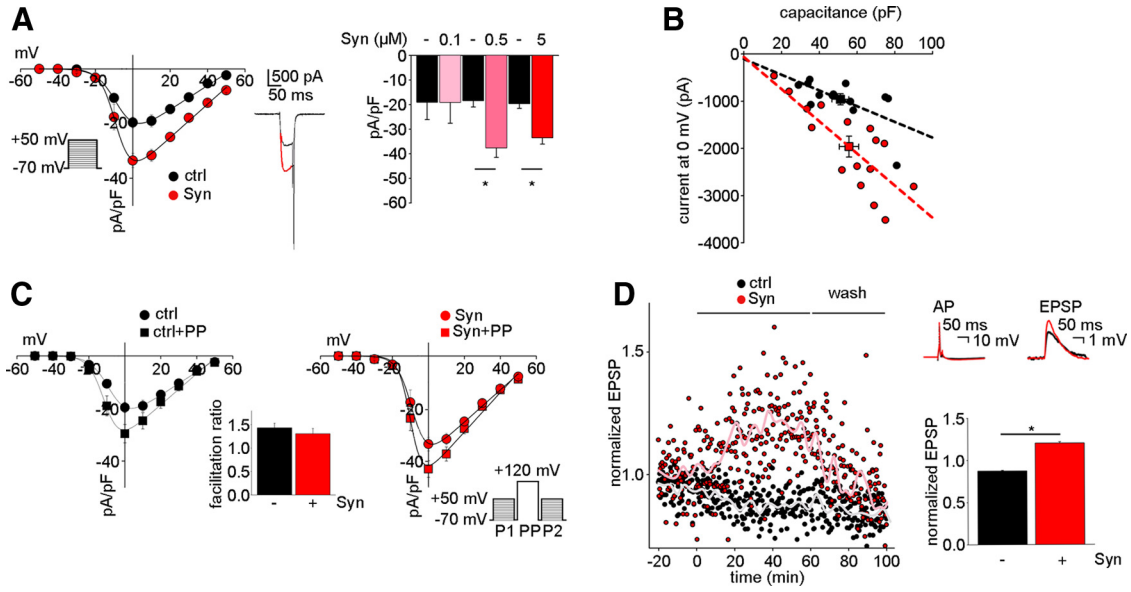

Figure 3. Extracellular Syn increases I_{Ba} currents and synaptic transmission in SCGNs. ***A***, Left, Mean calcium current density–voltage relationships for control (black circles; $n = 8$) and 5 μM Syn-treated (red circles; $n = 10$) SCGNs. Continuous lines are modified Boltzmann fits to each current density–voltage curve. Currents were evoked using 50 ms depolarizing test pulses in 10 mV intervals from a V_h of −70 mV. Data are shown as mean ± SEM. Middle, Superimposed representative traces showing currents at 0 mV in control (black) and after treatment with 5 μM Syn for 2 h (red). Right, Bar graph summarizing the effect of Syn on I_{Ba} and showing data for 0.1 μM Syn (light pink; $n = 5$), 0.5 μM (dark pink; $n = 6$), 5 μM (red; $n = 10$), and the respective controls (black; $n = 6, n = 6, n = 8$, respectively). Statistical significance determined by nonparametric *t* test. $^*p < 0.05$. ***B***, Plot of capacitance versus current at 0 mV recorded in SCGNs incubated with buffer (black circles; $n = 14$) or Syn (0.5 and 5 μM; red circles; $n = 16$). Dotted lines represent regression fits for buffer-treated (black) and Syn-treated (red) neurons. ***C***, Left, Superimposed current density–voltage curves showing I_{Ba} (P1; black circles) and effect of a depolarizing prepulse to +120 mV (P2; black squares) in control SCGNs used in ***A***. Right, Superimposed current density–voltage curves showing I_{Ba} (P1; red circles) and effect of a depolarizing prepulse to +120 mV (P2; red squares) in 5 μM Syn-treated SCGNs used in ***A***. Middle, Bar chart summarizing the facilitation ratio (P2/P1) expressed as the mean ± SEM in control (black) and 5 μM Syn-treated (red) SCGNs. ctrl, Control; PP, prepulse. ***D***, Left, EPSP amplitude evoked at 0.1 Hz in SCGN synapses. At $t = 0$ min, buffer (black circles; $n = 4$) or Syn (red circles; $n = 6$) were drop applied to the 2 ml bath (5 μM final concentration). EPSP amplitude was normalized to that before protein bath application for each neuron. The pink and gray lines represent smoothed values (10-point moving-average algorithm) of the EPSP amplitudes. Right, Top, Representative AP and EPSP traces measured at 40 min in control (black) and Syn-treated (red) SCGNs. Right, Bottom, Bar chart showing the increase of the normalized EPSP amplitude expressed as the mean ± SEM at $t = 40$ min in control (black) or Syn-treated (red) SCGNs. Statistical significance determined by nonparametric *t* test. $^*p < 0.05$.

Table 1. Effects of Syn on I_{Ba} current density

I–V	Current density at 0 mV (pA/pF)	G_{max} (nS/pF)	V_{rev} (mV)	*n*
Ctrl	−19.6 ± 2.0	0.33 ± 0.03	54.4 ± 3.4	8
Syn 5 μM	−33.5 ± 2.6*	0.56 ± 0.04*	61.5 ± 2.3	10
Ctrl	−18.4 ± 2.6	0.31 ± 0.04	54.6 ± 2.3	6
Syn 0.5 μM	−37.6 ± 3.9*	0.63 ± 0.07*	52.3 ± 1.5	6
Ctrl	−19.0 ± 7.1	0.32 ± 0.12	51.4 ± 1.3	6
Syn 0.1 μM	−19.1 ± 8.5	0.32 ± 0.14	53.6 ± 1.0	5

Current densities from control and Syn-treated SCG neurons were plotted against voltage and fitted with a single Boltzmann function. $^*p < 0.05$ versus control (Ctrl). Statistical significance for *I–V* data, expressed as mean ± SEM, was determined by Student's *t* test.

Table 2. Effect of 5 μM Syn on I_{Ba} parameters

Tail currents	*k* (mV)	$V_{0.5}$ (mV)	A1	*n*
Ctrl	12.1 ± 0.5	4.7 ± 2.0	0.98 ± 0.02	8
Syn 5 μM	8.0 ± 1.3*	0.2 ± 2.5	0.96 ± 0.02	10

Tail currents from control and Syn-treated SCGNs were plotted against voltage and fitted with a single Boltzmann function, as shown by single amplitude (A1) component values close to 1. $^*p < 0.05$ versus control (Ctrl). Data were expressed as mean ± SEM. Statistical significance was determined by nonparametric Mann–Whitney *U* test.

Table 3. Effects of PPF on Syn modulation of I_{Ba} current density

I–V	Current density at 0 mV (pA/pF)	V_{rev} (mV)	*n*
Ctrl	−19.6 ± 2.0	54.4 ± 3.4	8
Ctrl + PP	−29.6 ± 3.5*	51.8 ± 2.4	
Syn 5 μM	−33.5 ± 2.6*	61.5 ± 2.3	10
Syn 5 μM + PP	−43.0 ± 3.1**,***	58.5 ± 1.0	
Ctrl	−18.4 ± 2.6	54.6 ± 2.3	6
Ctrl + PP	−21.0 ± 2.4*	54.7 ± 2.7	
Syn 0.5 μM	−37.6 ± 3.9*	52.3 ± 1.5	6
Syn 0.5 μM + PP	−43.1 ± 5.6**,***	52.2 ± 1.1	
Ctrl	−19.0 ± 7.1	51.4 ± 1.3	6
Ctrl + PP	−22.1 ± 7.9*	52.5 ± 1.2	
Syn 0.1 μM	−19.1 ± 8.5	53.6 ± 1.0	5
Syn 0.1 μM + PP	−23.0 ± 9.1***	53.7 ± 1.1	

Current densities from control and SCGNs were plotted against voltage and fitted with a single Boltzmann function; prepulse (PP; to +120 mV). $^*p < 0.05$ versus control Ctrl); $^{**}p < 0.05$ versus control + PP; $^{***}p < 0.05$ versus Syn. Data were expressed as mean ± SEM. Statistical significance determined by Student's *t* test.

rule out any Syn-induced shift in voltage inactivation as the mechanism underlying the observed increase in calcium current density. The possibility that enhanced currents induced by Syn were attributable to an increase in the membrane surface of SCGNs was ruled out by capacitance measurement that revealed no changes between control and Syn-treated SCGNs with different current densities (Fig. 3*B*).

Calcium channels in SCGNs are physiologically modulated by voltage-dependent G-proteins (Dolphin, 1996), and G-protein modulation is characterized by an inhibition of current amplitude (Stephens et al., 1998). Therefore, we examined the effect of Syn on endogenous G-protein modulation. Transient dissociation of G-proteins from the channel induces facilitation of calcium currents that can be measured in response to a brief, strongly depolarizing voltage step [named prepulse facilitation (PPF)]. A prepulse of +120 mV was applied to control neurons to measure endogenous G-protein modulation (Fig. 3*C*; Table 3). In the control group (Fig. 3*C*, left; Table 3), the ratio between the currents recorded before (P1) and after (P2) the PPF step was 1.43 ± 0.10 ($n = 10$) at 0 mV. After pretreatment with 5 μM Syn (Fig. 3*C*, right; Table 3), the P2/P1 ratio was 1.31 ± 0.11 ($n = 10$)

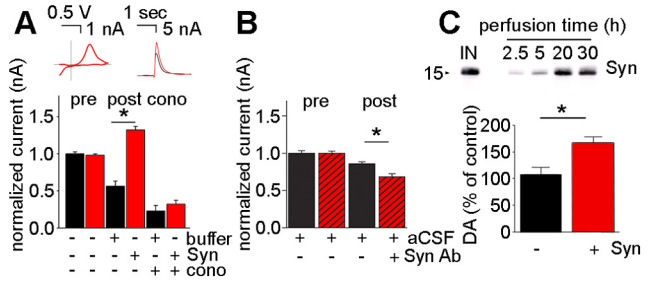

Figure 4. Syn increases DA release *ex vivo* and *in vivo*. ***A***, Fast-scan cyclic voltammograms of evoked DA release from striatal brain slices. Data were acquired every 2 min. At $t = 10$ min, buffer or 5 μM Syn was superfused. At $t = 30$ min, 25 nM ω-conotoxin was superfused for the remaining 20 min. Top, Representative voltammogram identifying the analyte as DA (left) and the amplitude of DA traces obtained during buffer (black) and Syn (red) superfusion (right). Bottom, Quantification of currents in control (black; $n = 2$) and Syn-treated (red; $n = 4$) slices before any addition (pre), during buffer or Syn treatment (post), and during ω-conotoxin (cono) treatment. Currents were normalized to the current in the first 10 min for each sample. Data were expressed as mean ± SEM. ***B***, Quantification of currents during the 10 min before any addition (pre) and during 10 min of treatment without or with 4 μg of anti-Syn antibody (Syn Ab) (post) in control (black; $n = 3$) and antibody perfused (red striped; $n = 3$) slices. Currents were normalized to the current in the first 10 min for each sample. Data were expressed as mean ± SEM. In ***A*** and ***B***, statistical significance was determined by two-way ANOVA for each condition. $^*p < 0.05$. ***C***, Top, Immunoblot showing the diffusion of Syn across the microdialysis membrane under *in vitro* conditions. Syn at 10 μM (IN) was added to the perfusion solution and perfused via a microdialysis cannula; samples of the external solution were collected at the indicated times. Bottom, Quantification of released DA measured by *in vivo* microdialysis in four awake animals during hour 3 of perfusion with buffer (black) or Syn (red). Data were expressed as percentage of DA level measured during perfusion with buffer, as mean ± SEM. Statistical significance determined by nonparametric *t* test. $^*p < 0.05$.

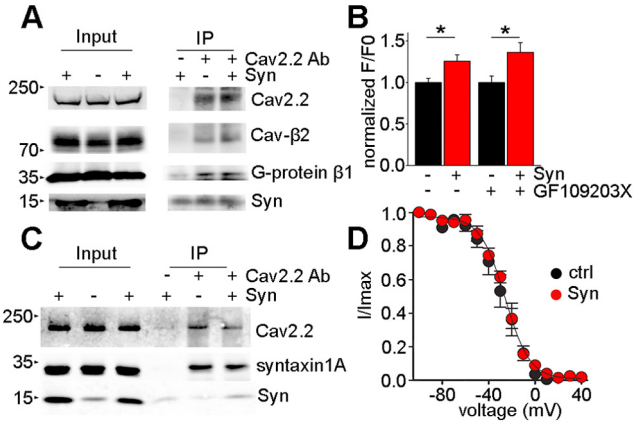

Figure 5. Syn does not alter modulation of $Ca_v2.2$ by interaction with major binding proteins. ***A***, Immunoblot showing coimmunoprecipitation with anti-$Ca_v2.2$ antibody ($Ca_v2.2$ Ab) from cortical neurons incubated with buffer (− Syn) or Syn (+ Syn) for 2 h at 37°C. The left three lanes show extracts (Input; 10% of the total). The right three lanes show immunoprecipitates (IP). Western blotting was performed with the antibodies indicated on the right. ***B***, Quantification of calcium transients in cortical neurons incubated with buffer (black) or Syn (red) for 2 h at 37°C. At 30 min before imaging, neurons were incubated with DMSO (−) or 1 μM GF109203X (+). Experiments were performed as in Figure 2*A*. $n = 100$ for each condition. Data are expressed as mean ± SEM of F/F_0 normalized to the respective control. Statistical significance determined by one-way ANOVA. $^*p < 0.05$. ***C***, Immunoblot showing coimmunoprecipitation with anti-$Ca_v2.2$ subunit antibody from cortical neurons incubated with buffer (− Syn) or Syn (+ Syn) for 2 h at 37°C, as described in ***A***. ***D***, Steady-state inactivation curves for control (ctrl; black circles; $n = 7$) and 5 μM Syn-treated (red circles; $n = 8$) SCGNs.

at 0 mV, showing that PPF of I_{Ba} caused a similar level of current relief from basal G-protein inhibition compared with controls (Fig. 3*C*, middle inset). Thus, together with the above, acutely isolated SCGNs exhibit enhanced calcium currents when pretreated with Syn, but Syn effects cannot be explained by a change in channel sensitivity to G-protein modulation.

We next investigated the modulatory role of Syn in synaptic transmission, taking advantage of the synapses formed among SCGNs in long-term culture (Fig. 3*D*). This is a well characterized model for studying fast cholinergic transmission and modulation of $Ca_v2.2$ (Mochida et al., 2003; Stephens and Mochida, 2005). Incubation of neurons with 5 μM Syn caused an increase in EPSP amplitude (Fig. 3*D*, left), with the maximum increase reached ~40 min after Syn application. The increase in synaptic transmission was reversible; washing out Syn from the bath returned synaptic transmission to control levels after an additional 40 min. These results indicate that Syn plays a modulatory role in evoked synchronous transmitter release, leading to an ~33% increase in EPSP amplitude compared with control (Fig. 3*D*, right). The observed effect of Syn on synaptic transmission is consistent with the reported increase in calcium current through presynaptic $Ca_v2.2$.

Syn-dependent activation of $Ca_v2.2$ leads to increased DA release in the striatum

Little is known about synaptic dysfunctions at the premanifest stage of PD. In mice overexpressing Syn, tonic DA release is increased at early stages of the pathology (Lam et al., 2011), and we show that Syn-dependent activation of $Ca_v2.2$ at the presynapse leads to altered neurotransmitter release in SCGNs. Increased extracellular DA may be a common mechanism contributing to substantia nigra dopaminergic neuron stress and eventual demise, subsequently leading to downregulation of synaptic activity in the striatum. To assess the effect of extracellular Syn on DA release in the striatum, we performed fast scan cyclic voltammetry experiments on striatal slices perfused with 5 μM purified Syn. Axonal DA release in the dorsolateral striatum was evoked using a twisted bipolar stimulating electrode. Stimulations were delivered every 2 min by a single electrical pulse (1 ms, 400 μA). Syn dissolved in aCSF was superfused 10 min after the first measure (control period), and, after 20 min of treatment, DA release increased by ~30% (Fig. 4*A*), in agreement with the observed increase in EPSP amplitude (Fig. 3*D*). Similarly to that observed for calcium entry, superfusion with ω-conotoxin primarily ablated DA release (Fig. 4*A*). ω-Conotoxin also reduced basal DA levels by ~60%, indicating that, in dorsolateral striatum preparations, $Ca_v2.2$ are the predominant calcium channels supporting neurotransmission (Phillips and Stamford, 2000). The large increase in DA release induced by excess Syn suggested a physiological role for Syn in the regulation of neurotransmitter release in the striatum. We wondered whether sequestration of constitutively released Syn from neurons would modify DA release in the opposite way. Perfusion of slices with anti-Syn antibody induced a significant ~10% decrease in DA release (Fig. 4*B*), indicating that Syn, in physiological conditions, acts as a positive regulator of neurotransmission.

To investigate the effect of *in vivo* acute administration of Syn on the release of DA in the striatum, we performed microdialysis to perfuse Syn in the striatum and measured DA released from the same area (Fig. 4*C*). The ability of Syn to diffuse through a microdialysis membrane with 100 kDa cutoff was determined under *in vitro* microdialysis conditions, and the passage of Syn into the solution outside the membrane was verified by immunoblot (Fig. 4*C*, top). Then, a 4-mm-long microdialysis cannula passing through the whole length of striatum was placed in the dorsal striatum of the rat. Freely moving rats were perfused at a rate of 0.25 μl/min with aCSF

solution with or without 10 μM Syn. Samples were collected for 60 min during hour 3 after addition of Syn into the perfusion solution and measured by HPLC. These experiments revealed a significant ~50% increase in DA release in the Syn-treated group compared with respective control values obtained during perfusion of solution without Syn (Fig. 4*C*, bottom).

Extracellular Syn does not affect $Ca_v2.2$ interaction with major regulatory proteins

$Ca_V2.2$ function is widely reported to be dictated by their interaction with a number of binding partners (Jarvis and Zamponi, 2007). Therefore, we investigated whether Syn directly binds $Ca_v2.2$ to affect their kinetics or indirectly affects other regulatory proteins. Neurons, incubated with 5 μM Syn for 2 h, were lysed and immunoprecipitated with anti-$Ca_v2.2$ antibody. Syn band was present also in the absence of anti-$Ca_v2.2$ antibody and in the absence of Syn addition because of unspecific binding of endogenous Syn to agarose beads, but it was not significantly increased in the anti-Cav2.2 + Syn sample (1.07 ± 0.19-fold vs control in the absence of Syn, $n = 3$), excluding a direct binding between the two proteins (Fig. 5*A*). To further evaluate the possibility that $Ca_v2.2$ activation was attributable to impaired binding of G-protein β1 subunit to the channel (Dolphin, 2003), we coimmunoprecipitated with anti-$Ca_v2.2$ antibody. The difference in the amount of G-protein β1 subunit coimmunoprecipitated with the channel in the presence of extracellular Syn was not significant (1.05 ± 0.11-fold vs control in the absence of Syn; $n = 3$; Fig. 5*A*), a result that is consistent with the observed lack of change in PPF in electrophysiological experiments. Furthermore, $Ca_v2.2$ is activated by protein kinase C (PKC; Stea et al., 1995), but in the presence of the PKC inhibitor GF109203X (2-[1-(3-dimethylaminopropyl)-1*H*-indol-3-yl]-3-(1*H*-indol-3-yl)maleimide) (Fig. 5*B*), there was no change in Syn-dependent increase in ω-conotoxin-sensitive calcium entry, excluding PKC as a mediator of Syn effect. To evaluate the possibility that Syn could induce a change in the binding of syntaxin 1A to $Ca_v2.2$ and remove the tonic inhibition of the channel (Davies et al., 2011), we analyzed the interaction between the two proteins in the absence or presence of Syn. No differences were observed between control and Syn-treated samples (1.03 ± 0.26-fold vs control in the absence of Syn; $n = 3$; Fig. 5*C*). Syntaxin 1A modulation of $Ca_V2.2$ has been reported to be associated with a stabilization of channel inactivation (Bezprozvanny et al., 1995). Consistent with a lack of effect on syntaxin 1A binding, Syn had no effect on $Ca_V2.2$ voltage dependence of inactivation (Fig. 5*D*).

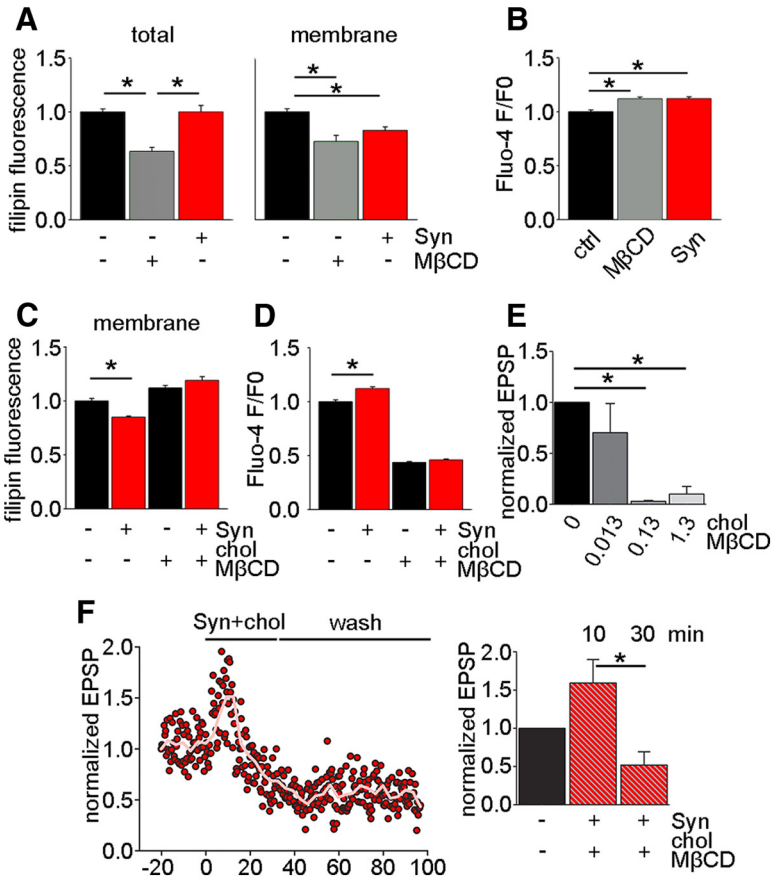

Figure 6. Syn acts on the content of plasma membrane cholesterol that affects calcium channel activation and neurotransmitter release. ***A***, Bar chart showing cholesterol levels determined by quantitative fluorescent filipin staining. Cortical neurons incubated with buffer (black), 1 mM MβCD (gray) or 5 μM Syn for 2 h (red), fixed and stained with filipin, with (left; total) or without (right; membrane) 0.1% Triton X-100. Bound filipin was extracted and quantified in a fluorometer. Mean fluorescence values from three different experiments each normalized to the respective controls. ***B***, Bar chart showing calcium transients in cortical neurons incubated with buffer (black), MβCD (green), or 5 μM Syn for 2 h (red). Experiments were performed as in Figure 2*A*. Data were expressed as normalized F/F_0 values. ***C***, Bar chart showing filipin fluorescence of cortical neurons incubated with buffer (black) or Syn (red) in the presence or absence of 1.3 mg/ml chol-MβCD for 2 h at 37°C. Neurons were fixed and stained as in ***A***, in the absence of detergents (membrane). ***D***, Bar chart showing calcium transients in cortical neurons incubated with buffer (black) or Syn (red) in the presence or absence of chol-MβCD. Experiments were performed as in Figure 2*A*. In ***A*** and ***C***, $n = 12$ for each condition; in ***B*** and ***D***, $n = 150$ for each condition. Data were expressed as mean ± SEM. Statistical significance determined by one-way ANOVA. $^*p < 0.05$. ***E***, Bar chart showing decrease of the EPSP amplitude normalized to the first 20 min before cholesterol addition (black), in chol-MβCD-treated SCGN synapses at $t = 10$ min (gray, at the concentrations indicated). ***F***, Left, Amplitude of EPSPs evoked at a frequency of 0.1 Hz in SCGN synapses. At $t = 0$ min, 5 μM Syn and chol-MβCD at 0.13 mg/ml (red dots; $n = 3$) were applied as in Figure 3*D*. EPSPs amplitude was normalized to the amplitude before protein bath application. Right, Bar chart showing the EPSP amplitude normalized to the first 20 min before any addition (black) in SCGN synapses treated with chol-MβCD and Syn (red/gray striped; $n = 3$) at $t = 10$ min and at $t = 30$ min. In ***E*** and ***F***, data were expressed as the mean ± SEM. Statistical significance determined by one-way ANOVA. $^*p < 0.05$. ctrl, Control.

Together, these data suggest that Syn neither binds directly to $Ca_V2.2$ nor acts by disrupting binding of effectors of major pathways incident on $Ca_V2.2$.

Extracellular Syn decreases plasma membrane cholesterol content

Ion channel activity is also widely reported to be regulated via the cholesterol content of the plasma membrane (Levitan et al., 2010), with calcium current shown to be decreased by cholesterol loading (Jennings et al., 1999; Toselli et al., 2005). Therefore, we measured total and plasma membrane cholesterol by staining with filipin, a cholesterol binding molecule, in permeabilized and nonpermeabilized neurons, respectively (Fig. 6*A*). Although methyl-β-cyclodextrin (MβCD), as expected, depleted both total

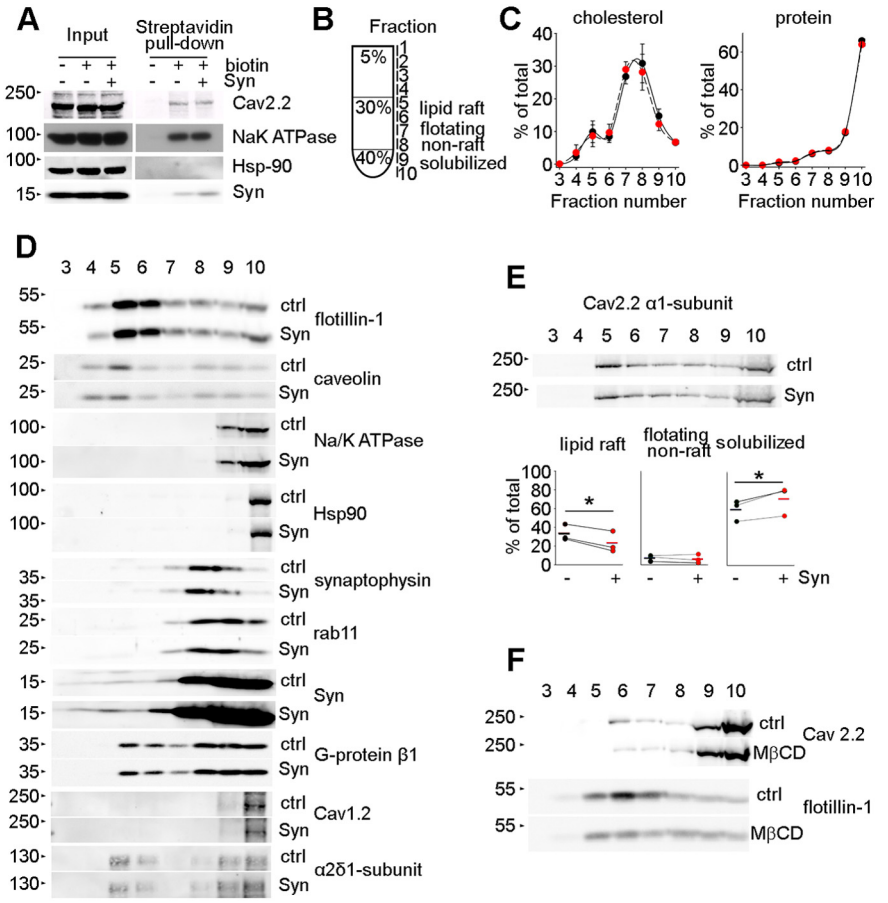

Figure 7. Separation of proteins by sucrose gradient. ***A***, Cell-surface biotinylation of cortical neurons incubated with buffer (− Syn) or Syn (+ Syn) for 2 h. The left three lanes show extracts (Input; 10% of the total). The right three lanes show nonbiotinylated (− biotin) and biotinylated (+ biotin) proteins pulled down with streptavidin beads. Western blotting was performed with the antibodies indicated on the right. ***B***, Schematic diagram of sucrose gradient fractionation. Cell extracts in 40% sucrose were placed at the bottom of the centrifuge tube and overlaid with 30% and 5% sucrose solutions. ***C***, Quantification of the cholesterol and protein content in the fractions collected from the gradient loaded with cortical neuron extracts incubated with buffer (black dots; $n = 3$) or Syn (red dots; $n = 3$) for 2 h. Data were expressed as percentage of the total cholesterol or protein content calculated as the sum of the content in each fraction. ***D***, Representative immunoblot of sucrose gradients loaded with extracts derived from neurons incubated with buffer (ctrl) or Syn (Syn), showing the distribution of proteins in raft (fractions 5 and 6; flotillin-1, caveolin, G-protein $\beta1$, $\alpha2\delta1$ subunit), flotating non-raft (fractions 7 and 8; synaptophysin, rab11, G-protein $\beta1$), and cholesterol-poor membranes (fractions 9 and 10; Na/K ATPase, Hsp90, $Ca_v1.2$). ***E***, Top, Sucrose gradient separation of proteins in lipid raft (5 and 6), flotating non-raft (7 and 8), and 1% Triton X-100 solubilized (9 and 10) components from cortical neurons incubated with buffer (ctrl) or Syn (Syn) for 2 h. Western blotting was performed with anti-$Ca_v2.2$ subunit. Bottom, Quantification by densitometry of protein content in the indicated fractions described above ($n = 3$). Data were expressed as percentage of the total protein amount calculated by the sum of the content of the protein of interest in each fraction. Statistical significance determined by paired *t* test. $^*p < 0.05$. ***F***, Immunoblot of sucrose gradients loaded with extracts derived from neurons incubated without (ctrl) or with 1.3 mg/ml MβCD, showing the distribution of proteins in raft, as described in ***D***.

and membrane cholesterol, Syn induced a selective ~30% decrease in plasma membrane cholesterol (Fig. 6*A*, right), whereas total cholesterol was unchanged. To assess the role of cholesterol on calcium influx in isolated cells, we used MβCD and cholesterol-loaded MβCD (chol-MβCD) to decrease and increase cholesterol content, respectively. We found that KCl-evoked calcium entry in the absence of calcium channel inhibitors was increased by MβCD, an effect mimicked by Syn (Fig. 6*B*), whereas in neurons loaded with cholesterol, evoked calcium entry was less than half of that in controls (Fig. 6*D*). We next investigated whether cholesterol loading of neurons could prevent Syn-induced depletion of plasma membrane cholesterol and calcium increase; indeed, both effects were blocked when neurons were incubated with chol-MβCD and Syn together (Fig. 6*C*,*D*). Together, these results indicate that a decrease in plasma membrane cholesterol content induced by extracellular Syn is causal to the increase in intracellular calcium. We next wondered whether cholesterol loading would act in the opposite manner to Syn and act to inhibit neurotransmitter release. SCGNs treated with 0.13 and 1.3 mg/ml chol-MβCD showed a dramatic reduction in EPSP amplitude compared with control (Fig. 6*E*). To monitor in real time the possible effect of cholesterol loading on Syn-driven increase in EPSP (Fig. 3*D*), we recorded EPSP from SCGNs loaded with chol-MβCD in the presence of Syn (Fig. 6*F*). The initial increase in amplitude was almost completely reversed after 20 min, with the effect of Syn decreasing to 40% of the initial value after 30 min. During washout, the reduction of EPSP amplitude persisted for the duration of the recording time (100 min; Fig. 6*F*), indicating that cholesterol loading strongly attenuated Syn effect on neurotransmission. Together, these results suggest a causal role for cholesterol in mediating Syn action.

$Ca_v2.2$ at the plasma membrane relocalize into cholesterol-poor domains during Syn action

An increased activity of $Ca_v2.2$ could be attributable to an increase in their surface expression. We characterized the amount of $Ca_v2.2$ by cell-surface biotinylation and found that Syn does not affect $Ca_v2.2$ expression at the neuronal plasma membrane (1.17 ± 0.10-fold vs control in the absence of Syn; $n = 4$; Fig. 7*A*). The reduced cholesterol level in the plasma membrane of neurons exposed to Syn was suggestive of a change in microdomain composition and partitioning of proteins. To address this hypothesis, we analyzed the potential changes in raft partitioning of different proteins in response to Syn treatment. Neuronal extracts were loaded at the bottom of a nonlinear sucrose gradient (Fig. 7*B*) and were shown to contain the same protein and cholesterol content in each fraction between control and Syn-treated neurons (Fig. 7*C*). It is well established that proteins, such as flotillin-1 and caveolin, represent markers for lipid rafts and partition into Triton X-100-insoluble cholesterol-rich microdomains (Bickel et al., 1997). In our gradient, flotillin-1 and caveolin were recovered in fractions 5 and 6 (Fig. 7*D*). Proteins that do not reside in cholesterol-rich domains, such as Na/K ATPase and Hsp90, are solubilized by Triton X-100 and were recovered in the non-flotating bottom fractions of the gradient (fractions 9 and 10; Fig. 7*D*). We found no significant differences in the distribution of the proteins analyzed in Figure 7*D*; however, during Syn incubation of neurons, $Ca_v2.2$ protein residing in the raft domains was decreased and its concentration was increased in the

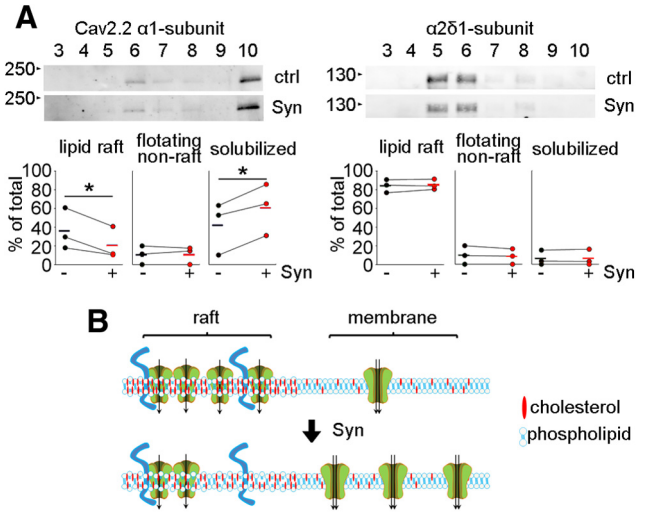

Figure 8. Syn induces relocalization of surface-exposed $Ca_v2.2$ in cholesterol-poor areas. ***A***, Cell-surface biotinylation followed by sucrose gradient separation of fractions as described in Figure 7*E*, from cortical neurons incubated with buffer (ctrl) or Syn (Syn) for 2 h. Western blotting was performed with anti-$Ca_v2.2$ subunit (left) and anti-$\alpha2\delta1$ subunit (right) antibodies. Bottom, Quantification by densitometry of protein content in the indicated fractions (as in Fig. 7*E*) collected from the gradient ($n = 3$). Statistical significance determined by paired *t* test. $^*p < 0.05$. ***B***, Diagram showing the partition of Ca_v 2.2 (green) that, in the presence of extracellular Syn, relocate into cholesterol (red)-poor domains of the plasma membrane, whereas $\alpha2\delta1$ subunit (blue) remains in raft domains. The relocalization of Ca_v 2.2 correlates with increased channel activity (double black arrows).

fraction containing solubilized proteins (Fig. 7*E*). As a control for cholesterol depletion, we treated neurons with MβCD and then loaded extracts on a sucrose gradient (Fig. 7*F*). However, MβCD primarily depletes cholesterol both inside the cell and at the membrane (Fig. 6*A*) and, as expected, induced an almost complete solubilization of $Ca_v2.2$ and also of proteins tightly associated with lipid rafts, such as flotillin-1.

Finally, we examined the behavior of surface exposed $Ca_v2.2$, whose activity accounted for the increased calcium currents observed in the presence of Syn above. We found that ~40% of the biotinylated channels that were in rafts in control conditions shifted to cholesterol-poor domains of the plasma membrane during Syn incubation (Fig. 8*A*, left); in contrast, α2δ-1 subunits, which also partition in lipid rafts and are widely reported to modulate trafficking and to direct Ca_v2 into lipid rafts (Davies et al., 2006; Robinson et al., 2010), remained in cholesterol-rich domains (Fig. 8*A*, right). These data indicate that the presence of extracellular Syn cause a relocation of cell-surface $Ca_v2.2$ into cholesterol-poor domains of the plasma membrane (Fig. 8*B*). This change in the environment of the channel is consistent with increased channel activation, calcium entry, and release of neurotransmitters.

Discussion

Our study focuses on the pathological role of increased concentrations of extracellular Syn, a condition that might arise by the release of Syn from neurons in which Syn is overexpressed, because of the presence of multiple *SNCA* gene copies (Singleton et al., 2003; Farrer et al., 2004) or polymorphism in regions of the gene that regulate its expression (Chiba-Falek et al., 2006). Our results provide evidence that Syn alters the organization of the plasma membrane of neurons, acting on the external leaflet of the membrane to lower the content of plasma membrane cholesterol and thereby altering the partitioning of surface-associated proteins. Syn action leads to increased presynaptic calcium influx and neurotransmitter release mediated by $Ca_V2.2$. There is much evidence that Syn function is related to its association with plasma and vesicular membranes at synaptic terminals (Sharon et al., 2001) and in particular with lipid rafts (Fortin et al., 2004). *In vitro* studies suggest an effect of Syn on the integrity of lipid bilayers inducing lipid clustering (Madine et al., 2006). It was shown recently in SH-SY5Y cells that membrane fluidity was affected by exogenous Syn (Melachroinou et al., 2013). The observed effect of Syn on the composition of plasma membrane may involve altered endocytosis or recycling of lipid and proteins, leading to incorrect positioning of proteins in microdomains with different lipid composition, rather than causing differences in the amount of proteins at the cell surface. In our study, an effect of Syn on membrane retrieval to the intracellular compartment was ruled out by the measurements of capacitance, which appeared unchanged. However, it is possible that membrane retrieval of raft domains is accompanied by recycling of cholesterol-poor vesicles at the membrane, leaving the surface area intact. In particular, we found that $Ca_v2.2$ repositioned in cholesterol-poor domains with important effects on channel electrophysiological properties. The reported reduction in slope factor from calcium tail current amplitude measurements suggests an improvement of channel voltage sensitivity, such that the gating charges move more easily and, thus, that channel activation is improved. The large increase in current conductance with an accompanying improved voltage sensitivity of the channel is likely a result of the compartmentalization of the channel in less stiffer membrane domains in which the membrane deformation energy required for the transition from closed to open state is lower (Lundbaek et al., 1996; Levitan et al., 2000). It has been shown that lipid rafts composition affects calcium channels currents (Davies et al., 2006; Levitan et al., 2010). In neuroblastoma × glioma NG-108 hybrid cells, cholesterol loading selectively reduces $Ca_v2.2$ currents by decreasing the channel open probability (Toselli et al., 2005). Conversely, cholesterol depletion by MβCD, which disrupts lipid rafts, has been shown to induce increase $Ca_V2.1$ current in recombinant cells (Davies et al., 2006) and to cause a trend to increase current in caveolin-1 transfected NG-108 cells (Toselli et al., 2005). These reports suggest that association of $Ca_V2.2$ in a lipid-rich environment results in reduced calcium current, whereas in a lower cholesterol environment, current is increased. Here we show that, in both central and peripheral neurons, cholesterol depletion mimics Syn action and that cholesterol loading has opposite effects to Syn on synaptic transmission. The improved transition between the closed and open states of the channels in a cholesterol-poor environment seems independent of the association of the channel with α2δ-1 subunit on the surface. Thus, the localization of surface α2δ-1 subunit, highly enriched in raft domains (Robinson et al., 2010), was unaffected by the presence of Syn. α2δ subunits control the functional expression of the α1 subunit, modulating its trafficking from the cell soma and leading to a significant increase in synaptic abundance of α1 (Dolphin, 2009). The comparable amount of surface-exposed $Ca_v2.2$ in control and Syn-treated neurons indicated that α2δ-1-dependent trafficking of channels to the membrane was unchanged. Overall, we demonstrate that the Syn-mediated shift of $Ca_v2.2$ into cholesterol-poor domains is sufficient to induce enhancement of calcium current independently of α2δ association with the channel.

Our data suggest that, in the presence of Syn, channels are shifted into a low-cholesterol environment, and the ensuing increase in calcium influx has a profound effect on release. It has

been shown that cholesterol depletion does not influence the confinement of Ca_v1 in proximity to release sites at bipolar cells ribbon synapses (Thoreson et al., 2013), suggesting that lipid rafts are not required to cluster Ca_v1, but rather clusters of channels are maintained by interaction with presynaptic proteins and cytoskeletal elements. Effects may be synapse specific, in that the same group reports that cholesterol depletion does affect Ca_v1 channel mobility at photoreceptor synapses in the retina (Mercer et al., 2011, 2012). Importantly, in these studies, Ca_v1 channel mobility was assessed via the use of antibodies against the major retinal α2δ-4 subunit. It may be that α2δ subunits are important for trafficking of $Ca_v2.2$ from the endoplasmic reticulum to the plasma membrane (Dolphin, 2012), but once at the membrane, association is more labile, consistent with reported low-affinity association of α2δ with $Ca_v2.2$ in plasma membrane proteomic studies (Muller et al., 2010). As above, our data strongly suggest that Syn effects on release occur in the absence of movement of α2δ-1, which we show to be retained in cholesterol-rich domains. Therefore, it is possible that, during exposure to Syn, $Ca_v2.2$, independently from α2δ-1 and lipid rafts, remain positioned at lower cholesterol regions within active zones in which they sustain neurotransmitter release. It is also reported that cholesterol depletion decreases synaptic vesicles release by altering membrane curvature (Rituper et al., 2013). However, extracellular Syn did not affect internal cholesterol levels here, arguing against a major contribution to effects on release in this study. Another possible explanation for the observed increase in $Ca_v2.2$ activity is that changes in membrane organization may move the channels into proximity of a second messenger, such as phosphatidylinositol 4,5-bisphosphate, which in turn modulates channel activity (Roberts-Crowley et al., 2009). The importance of $Ca_v2.2$ in neurotransmission at the presynapse is well documented, and these channels are the main players in the control of striatal DA release (Phillips and Stamford, 2000). We provide evidence that DA release is significantly increased in a ω-conotoxin-sensitive manner in striatal slices superfused with Syn, and this result correlates with the increase in calcium entry at the presynapse, as assessed by the use of SyGCaMP3. Together, these data identify a mechanism that would explain the increase in DA release found at premanifest stages of PD in Syn transgenic mice (Lam et al., 2011) and in virus-injected mice at early stages of the pathology (Chung et al., 2009). The increase in DA is reproduced *in vivo* by microdialysis of Syn directly into the striatum, suggesting a tonic increase in DA levels attributable to Syn accumulation in the synaptic cleft. Early alterations at the synaptic terminals level might be responsible for the "dying back" of dopaminergic neurons starting at the axon terminal, sensitizing DA neurons in the initial, presymptomatic, stages of disease. The underlying regulatory mechanism we propose—Syn-mediated disorganization of lipid rafts (Fig. 8*B*)—may also occur in other areas prone to neurodegeneration in PD and affect the function of other plasma membrane-associated proteins, possibly explaining the selective vulnerability of particular subset of neurons depending on their lipid and protein composition. As an example, the $Ca_v2.2$ knockout mice model displays reduction in pain sensitivity (Saegusa et al., 2002), and pain is one of the non-motor symptoms of PD; therefore, we can speculate a causal relationship between hyperactivation of Cav2.2 and pain sensitivity in PD.

References

Adamczyk A, Strosznajder JB (2006) Alpha-synuclein potentiates Ca2+ influx through voltage-dependent Ca2+ channels. Neuroreport 17:1883–1886. CrossRef Medline

Bergquist F, Jonason J, Pileblad E, Nissbrandt H (1998) Effects of local administration of L-, N-, and P/Q-type calcium channel blockers on spontaneous dopamine release in the striatum and the substantia nigra: a microdialysis study in rat. J Neurochem 70:1532–1540. CrossRef Medline

Bezprozvanny I, Scheller RH, Tsien RW (1995) Functional impact of syntaxin on gating of N-type and Q-type calcium channels. Nature 378:623–626. CrossRef Medline

Bickel PE, Scherer PE, Schnitzer JE, Oh P, Lisanti MP, Lodish HF (1997) Flotillin and epidermal surface antigen define a new family of caveolae-associated integral membrane proteins. J Biol Chem 272:13793–13802. CrossRef Medline

Borghi R, Marchese R, Negro A, Marinelli L, Forloni G, Zaccheo D, Abbruzzese G, Tabaton M (2000) Full length alpha-synuclein is present in cerebrospinal fluid from Parkinson's disease and normal subjects. Neurosci Lett 287:65–67. CrossRef Medline

Brewer GJ (1997) Isolation and culture of adult rat hippocampal neurons. J Neurosci Methods 71:143–155. CrossRef Medline

Bucci G, Mochida S, Stephens GJ (2011) Inhibition of synaptic transmission and G protein modulation by synthetic CaV2.2 Ca(2)+ channel peptides. J Physiol 589:3085–3101. CrossRef Medline

Butchbach ME, Tian G, Guo H, Lin CL (2004) Association of excitatory amino acid transporters, especially EAAT2, with cholesterol-rich lipid raft microdomains: importance for excitatory amino acid transporter localization and function. J Biol Chem 279:34388–34396. CrossRef Medline

Catterall WA (2000) Structure and regulation of voltage-gated Ca2+ channels. Annu Rev Cell Dev Biol 16:521–555. CrossRef Medline

Chiba-Falek O, Lopez GJ, Nussbaum RL (2006) Levels of alpha-synuclein mRNA in sporadic Parkinson disease patients. Mov Disord 21:1703–1708. CrossRef Medline

Chung CY, Koprich JB, Siddiqi H, Isacson O (2009) Dynamic changes in presynaptic and axonal transport proteins combined with striatal neuroinflammation precede dopaminergic neuronal loss in a rat model of AAV α-synucleinopathy. J Neurosci 29:3365–3373. CrossRef Medline

Crowet JM, Lins L, Dupiereux I, Elmoualija B, Lorin A, Charloteaux B, Stroobant V, Heinen E, Brasseur R (2007) Tilted properties of the 67–78 fragment of alpha-synuclein are responsible for membrane destabilization and neurotoxicity. Proteins 68:936–947. CrossRef Medline

Damier P, Hirsch EC, Agid Y, Graybiel AM (1999) The substantia nigra of the human brain. I. Nigrosomes and the nigral matrix, a compartmental organization based on calbindin D(28K) immunohistochemistry. Brain 122:1421–1436. CrossRef Medline

Davies A, Douglas L, Hendrich J, Wratten J, Tran Van Minh A, Foucault I, Koch D, Pratt WS, Saibil HR, Dolphin AC (2006) The calcium channel alpha2delta-2 subunit partitions with CaV2.1 into lipid rafts in cerebellum: implications for localization and function. J Neurosci 26:8748–8757. CrossRef Medline

Davies JN, Jarvis SE, Zamponi GW (2011) Bipartite syntaxin 1A interactions mediate CaV2.2 calcium channel regulation. Biochem Biophys Res Commun 411:562–568. CrossRef Medline

Decressac M, Mattsson B, Lundblad M, Weikop P, Björklund A (2012) Progressive neurodegenerative and behavioural changes induced by AAV-mediated overexpression of alpha-synuclein in midbrain dopamine neurons. Neurobiol Dis 45:939–953. CrossRef Medline

Dodge FA Jr, Rahamimoff R (1967) On the relationship between calcium concentration and the amplitude of the end-plate potential. J Physiol 189:90P–92P. Medline

Dolphin AC (1996) Facilitation of Ca2+ current in excitable cells. Trends Neurosci 19:35–43. CrossRef Medline

Dolphin AC (2003) G protein modulation of voltage-gated calcium channels. Pharmacol Rev 55:607–627. CrossRef Medline

Dolphin AC (2009) Calcium channel diversity: multiple roles of calcium channel subunits. Curr Opin Neurobiol 19:237–244. CrossRef Medline

Dolphin AC (2012) Calcium channel auxiliary alpha2delta and beta subunits: trafficking and one step beyond. Nat Rev Neurosci 13:542–555. CrossRef Medline

El-Agnaf OM, Salem SA, Paleologou KE, Cooper LJ, Fullwood NJ, Gibson MJ, Curran MD, Court JA, Mann DM, Ikeda S, Cookson MR, Hardy J, Allsop D (2003) Alpha-synuclein implicated in Parkinson's disease is present in extracellular biological fluids, including human plasma. FASEB J 17:1945–1947. CrossRef Medline

Fantini J, Carlus D, Yahi N (2011) The fusogenic tilted peptide (67–78) of alpha-synuclein is a cholesterol binding domain. Biochim Biophys Acta 1808:2343–2351. CrossRef Medline

Farrer M, Kachergus J, Forno L, Lincoln S, Wang DS, Hulihan M, Maraganore D, Gwinn-Hardy K, Wszolek Z, Dickson D, Langston JW (2004) Comparison of kindreds with parkinsonism and alpha-synuclein genomic multiplications. Ann Neurol 55:174–179. CrossRef Medline

Fortin DL, Troyer MD, Nakamura K, Kubo S, Anthony MD, Edwards RH (2004) Lipid rafts mediate the synaptic localization of α-synuclein. J Neurosci 24:6715–6723. CrossRef Medline

Garner CC, Kindler S, Gundelfinger ED (2000) Molecular determinants of presynaptic active zones. Curr Opin Neurobiol 10:321–327. CrossRef Medline

Goldberg MS, Fleming SM, Palacino JJ, Cepeda C, Lam HA, Bhatnagar A, Meloni EG, Wu N, Ackerson LC, Klapstein GJ, Gajendiran M, Roth BL, Chesselet MF, Maidment NT, Levine MS, Shen J (2003) Parkin-deficient mice exhibit nigrostriatal deficits but not loss of dopaminergic neurons. J Biol Chem 278:43628–43635. CrossRef Medline

Hansen C, Angot E, Bergström AL, Steiner JA, Pieri L, Paul G, Outeiro TF, Melki R, Kallunki P, Fog K, Li JY, Brundin P (2011) alpha-Synuclein propagates from mouse brain to grafted dopaminergic neurons and seeds aggregation in cultured human cells. J Clin Invest 121:715–725. CrossRef Medline

Hell JW, Westenbroek RE, Breeze LJ, Wang KK, Chavkin C, Catterall WA (1996) *N*-methyl-D-aspartate receptor-induced proteolytic conversion of postsynaptic class C L-type calcium channels in hippocampal neurons. Proc Natl Acad Sci U S A 93:3362–3367. CrossRef Medline

Hettiarachchi NT, Parker A, Dallas ML, Pennington K, Hung CC, Pearson HA, Boyle JP, Robinson P, Peers C (2009) alpha-Synuclein modulation of Ca2+ signaling in human neuroblastoma (SH-SY5Y) cells. J Neurochem 111:1192–1201. CrossRef Medline

Jarvis SE, Zamponi GW (2007) Trafficking and regulation of neuronal voltage-gated calcium channels. Curr Opin Cell Biol 19:474–482. CrossRef Medline

Jennings LJ, Xu QW, Firth TA, Nelson MT, Mawe GM (1999) Cholesterol inhibits spontaneous action potentials and calcium currents in guinea pig gallbladder smooth muscle. Am J Physiol 277:G1017–G1026. Medline

Kim BG, Shin DH, Jeon GS, Seo JH, Kim YW, Jeon BS, Cho SS (2000) Relative sparing of calretinin containing neurons in the substantia nigra of 6-OHDA treated rat Parkinsonian model. Brain Res 855:162–165. CrossRef Medline

Kordower JH, Chu Y, Hauser RA, Freeman TB, Olanow CW (2008a) Lewy body-like pathology in long-term embryonic nigral transplants in Parkinson's disease. Nat Med 14:504–506. CrossRef Medline

Kordower JH, Chu Y, Hauser RA, Olanow CW, Freeman TB (2008b) Transplanted dopaminergic neurons develop PD pathologic changes: a second case report. Mov Disord 23:2303–2306. CrossRef Medline

Kuhr WG, Wightman RM (1986) Real-time measurement of dopamine release in rat brain. Brain Res 381:168–171. CrossRef Medline

Laemmli UK (1970) Cleavage of structural proteins during the assembly of the head of bacteriophage T4. Nature 227:680–685. CrossRef Medline

Lam HA, Wu N, Cely I, Kelly RL, Hean S, Richter F, Magen I, Cepeda C, Ackerson LC, Walwyn W, Masliah E, Chesselet MF, Levine MS, Maidment NT (2011) Elevated tonic extracellular dopamine concentration and altered dopamine modulation of synaptic activity precede dopamine loss in the striatum of mice overexpressing human alpha-synuclein. J Neurosci Res 89:1091–1102. CrossRef Medline

Levitan I, Christian AE, Tulenko TN, Rothblat GH (2000) Membrane cholesterol content modulates activation of volume-regulated anion current in bovine endothelial cells. J Gen Physiol 115:405–416. CrossRef Medline

Levitan I, Fang Y, Rosenhouse-Dantsker A, Romanenko V (2010) Cholesterol and ion channels. Subcell Biochem 51:509–549. CrossRef Medline

Li H, Foss SM, Dobryy YL, Park CK, Hires SA, Shaner NC, Tsien RY, Osborne LC, Voglmaier SM (2011) Concurrent imaging of synaptic vesicle recycling and calcium dynamics. Front Mol Neurosci 4:34. CrossRef Medline

Lundbaek JA, Birn P, Girshman J, Hansen AJ, Andersen OS (1996) Membrane stiffness and channel function. Biochemistry 35:3825–3830. CrossRef Medline

Lundblad M, Decressac M, Mattsson B, Björklund A (2012) Impaired neurotransmission caused by overexpression of alpha-synuclein in nigral dopamine neurons. Proc Natl Acad Sci U S A 109:3213–3219. CrossRef Medline

Madine J, Doig AJ, Middleton DA (2006) A study of the regional effects of alpha-synuclein on the organization and stability of phospholipid bilayers. Biochemistry 45:5783–5792. CrossRef Medline

Martinez J, Moeller I, Erdjument-Bromage H, Tempst P, Lauring B (2003) Parkinson's disease-associated alpha-synuclein is a calmodulin substrate. J Biol Chem 278:17379–17387. CrossRef Medline

Mattson MP (2007) Calcium and neurodegeneration. Aging Cell 6:337–350. CrossRef Medline

Melachroinou K, Xilouri M, Emmanouilidou E, Masgrau R, Papazafiri P, Stefanis L, Vekrellis K (2013) Deregulation of calcium homeostasis mediates secreted alpha-synuclein-induced neurotoxicity. Neurobiol Aging 34:2853–2865. CrossRef Medline

Mercer AJ, Chen M, Thoreson WB (2011) Lateral mobility of presynaptic L-type calcium channels at photoreceptor ribbon synapses. J Neurosci 31:4397–4406. CrossRef Medline

Mercer AJ, Szalewski RJ, Jackman SL, Van Hook MJ, Thoreson WB (2012) Regulation of presynaptic strength by controlling Ca2+ channel mobility: effects of cholesterol depletion on release at the cone ribbon synapse. J Neurophysiol 107:3468–3478. CrossRef Medline

Mochida S, Sheng ZH, Baker C, Kobayashi H, Catterall WA (1996) Inhibition of neurotransmission by peptides containing the synaptic protein interaction site of N-type Ca2+ channels. Neuron 17:781–788. CrossRef Medline

Mochida S, Westenbroek RE, Yokoyama CT, Itoh K, Catterall WA (2003) Subtype-selective reconstitution of synaptic transmission in sympathetic ganglion neurons by expression of exogenous calcium channels. Proc Natl Acad Sci U S A 100:2813–2818. CrossRef Medline

Müller CS, Haupt A, Bildl W, Schindler J, Knaus HG, Meissner M, Rammner B, Striessnig J, Flockerzi V, Fakler B, Schulte U (2010) Quantitative proteomics of the Cav2 channel nano-environments in the mammalian brain. Proc Natl Acad Sci U S A 107:14950–14957. CrossRef Medline

Niwa H, Yamamura K, Miyazaki J (1991) Efficient selection for high-expression transfectants with a novel eukaryotic vector. Gene 108:193–199. CrossRef Medline

Nuber S, Harmuth F, Kohl Z, Adame A, Trejo M, Schönig K, Zimmermann F, Bauer C, Casadei N, Giel C, Calaminus C, Pichler BJ, Jensen PH, Müller CP, Amato D, Kornhuber J, Teismann P, Yamakado H, Takahashi R, Winkler J, et al. (2013) A progressive dopaminergic phenotype associated with neurotoxic conversion of alpha-synuclein in BAC-transgenic rats. Brain 136:412–432. CrossRef Medline

Phillips PE, Stamford JA (2000) Differential recruitment of N-, P- and Q-type voltage-operated calcium channels in striatal dopamine release evoked by "regular" and "burst" firing. Brain Res 884:139–146. CrossRef Medline

Rituper B, Chowdhury HH, Jorgacevski J, Coorssen JR, Kreft M, Zorec R (2013) Cholesterol-mediated membrane surface area dynamics in neuroendocrine cells. Biochim Biophys Acta 1831:1228–1238. CrossRef Medline

Roberts-Crowley ML, Mitra-Ganguli T, Liu L, Rittenhouse AR (2009) Regulation of voltage-gated Ca2+ channels by lipids. Cell Calcium 45:589–601. CrossRef Medline

Robinson P, Etheridge S, Song L, Armenise P, Jones OT, Fitzgerald EM (2010) Formation of N-type (Cav2.2) voltage-gated calcium channel membrane microdomains: lipid raft association and clustering. Cell Calcium 48:183–194. CrossRef Medline

Saegusa H, Matsuda Y, Tanabe T (2002) Effects of ablation of N- and R-type Ca(2+) channels on pain transmission. Neurosci Res 43:1–7. CrossRef Medline

Satake W, Nakabayashi Y, Mizuta I, Hirota Y, Ito C, Kubo M, Kawaguchi T, Tsunoda T, Watanabe M, Takeda A, Tomiyama H, Nakashima K, Hasegawa K, Obata F, Yoshikawa T, Kawakami H, Sakoda S, Yamamoto M, Hattori N, Murata M, Nakamura Y, et al. (2009) Genome-wide association study identifies common variants at four loci as genetic risk factors for Parkinson's disease. Nat Genet 41:1303–1307. CrossRef Medline

Sharon R, Goldberg MS, Bar-Josef I, Betensky RA, Shen J, Selkoe DJ (2001) alpha-Synuclein occurs in lipid-rich high molecular weight complexes, binds fatty acids, and shows homology to the fatty acid-binding proteins. Proc Natl Acad Sci U S A 98:9110–9115. CrossRef Medline

Singleton AB, Farrer M, Johnson J, Singleton A, Hague S, Kachergus J, Hulihan M, Peuralinna T, Dutra A, Nussbaum R, Lincoln S, Crawley A, Hanson M, Maraganore D, Adler C, Cookson MR, Muenter M, Baptista M,

Miller D, Blancato J, et al. (2003) alpha-Synuclein locus triplication causes Parkinson's disease. Science 302:841. CrossRef Medline

Soós J, Engelhardt JI, Siklós L, Havas L, Majtényi K (2004) The expression of PARP, NF-kappa B and parvalbumin is increased in Parkinson disease. Neuroreport 15:1715–1718. CrossRef Medline

Spillantini MG, Schmidt ML, Lee VM, Trojanowski JQ, Jakes R, Goedert M (1997) Alpha-synuclein in Lewy bodies. Nature 388:839–840. CrossRef Medline

Stea A, Soong TW, Snutch TP (1995) Determinants of PKC-dependent modulation of a family of neuronal calcium channels. Neuron 15:929–940. CrossRef Medline

Stephens GJ, Mochida S (2005) G protein {beta}{gamma} subunits mediate presynaptic inhibition of transmitter release from rat superior cervical ganglion neurones in culture. J Physiol 563:765–776. CrossRef Medline

Stephens GJ, Brice NL, Berrow NS, Dolphin AC (1998) Facilitation of rabbit alpha1B calcium channels: involvement of endogenous Gbetagamma subunits. J Physiol 509:15–27. CrossRef Medline

Stoehr SJ, Campbell GW, Rock DM (1997) Evaluation of N-type Ca2+ channel currents in cultured rat superior cervical ganglion neurons. Drug Dev Res 41:85–90. CrossRef

Thoreson WB, Mercer AJ, Cork KM, Szalewski RJ (2013) Lateral mobility of L-type calcium channels in synaptic terminals of retinal bipolar cells. Mol Vis 19:16–24. Medline

Toselli M, Biella G, Taglietti V, Cazzaniga E, Parenti M (2005) Caveolin-1 expression and membrane cholesterol content modulate N-type calcium channel activity in NG108–15 cells. Biophys J 89:2443–2457. CrossRef Medline

Venda LL, Cragg SJ, Buchman VL, Wade-Martins R (2010) alpha-Synuclein and dopamine at the crossroads of Parkinson's disease. Trends Neurosci 33:559–568. CrossRef Medline

Volpicelli-Daley LA, Luk KC, Patel TP, Tanik SA, Riddle DM, Stieber A, Meaney DF, Trojanowski JQ, Lee VM (2011) Exogenous alpha-synuclein fibrils induce Lewy body pathology leading to synaptic dysfunction and neuron death. Neuron 72:57–71. CrossRef Medline

Walsh DM, Selkoe DJ (2004) Deciphering the molecular basis of memory failure in Alzheimer's disease. Neuron 44:181–193. CrossRef Medline

Westenbroek RE, Hell JW, Warner C, Dubel SJ, Snutch TP, Catterall WA (1992) Biochemical properties and subcellular distribution of an N-type calcium channel alpha 1 subunit. Neuron 9:1099–1115. CrossRef Medline

Wu N, Joshi PR, Cepeda C, Masliah E, Levine MS (2010) Alpha-synuclein overexpression in mice alters synaptic communication in the corticostriatal pathway. J Neurosci Res 88:1764–1776. CrossRef Medline